Interfacial properties between CoO (100) and Fe_3O_4 (100)

Hui-Qiong Wang,[1,3] Eric I. Altman,[2,3] and Victor E. Henrich[1,3]
[1]*Department of Applied Physics, Yale University, P.O. Box 208284, New Haven, Connecticut 06520, USA*
[2]*Department of Chemical Engineering, Yale University, P.O. Box 208284, New Haven, Connecticut 06520, USA*
[3]*Center for Research on Interface Structures and Phenomena (CRISP), Yale University, P.O. Box 208284, New Haven, Connecticut 06520, USA*

(Received 21 October 2007; revised manuscript received 19 January 2008; published 19 February 2008)

Using molecular beam epitaxy 1–20 ML thick CoO (100) films were grown monolayer by monolayer on Fe_3O_4 (100) substrates. The stoichiometry of the films was verified by low-energy-electron diffraction and reflection-high-energy-electron diffraction patterns, as well as x-ray photoelectron spectroscopy. Auger measurements as a function of CoO film thickness indicated a layer-by-layer growth mode. Ultraviolet photoelectron spectroscopy (UPS) was used to monitor the thin film electronic properties. The evolution of the density of states in the O $2p$/Fe $3d$ and O $2p$/Co $3d$ bands exhibits a shift in the position of the CoO valence band for ultrathin films relative to bulklike thick films. The measured spectra (when aligned to cancel the band shift) are compared to models of the spectra that would be expected based on the bulk compounds, with and without additional interfacial electronic states. Electronic states at the Fe_3O_4-CoO interface have been identified, and their UPS spectrum has been determined.

DOI: 10.1103/PhysRevB.77.085313 PACS number(s): 73.20.−r, 79.60.Jv, 79.60.Dp

I. INTRODUCTION

The growth of one oxide thin film on another oxide is a research field of intense current interest. Of particular interest is film growth involving Fe_3O_4, which is motivated by the all-oxide spin valves proposed utilizing the half-metallic character of Fe_3O_4.[1] Fe_3O_4-CoO has been proposed as a component in such a tunneling device.[1] The system is also interesting because the interface is between a metallic inverse spinel ferrimagnet (Fe_3O_4) and an insulating rocksalt antiferromagnet (CoO). Although the two oxides have different crystal structures, they share the same face-centered cubic (fcc) oxygen sublattice. While Fe_3O_4 has a lattice constant of 8.396 Å, nearly twice of that of CoO (4.26 Å), they both have the same square arrangement of oxygen ions on their (100) faces; the sizes of the primitive unit cells of the O sublattices differ by only 1.45%. In addition, the oxygen affinities of FeO and Co—the first reduction species for the two oxides—are comparable.[2] Therefore, when Co atoms are deposited onto Fe_3O_4, they will not tend to reduce the iron oxide and thus the interface should be fairly chemically inert. All these features, in principle, make it easy to fabricate the Fe_3O_4-CoO interface, similar to the Fe_3O_4-NiO interface.[3]

The Fe_3O_4-CoO system exhibits the exchange biasing effect,[4,5] in which the hysteresis loop of a ferro- or ferrimagnet is shifted asymmetrically along the field axis when the ferromagnetic material is in contact with an antiferromagnetic material, due to magnetic interactions across the oxide-oxide interface; this effect is also observed in the Fe_3O_4-NiO system.[6] Such an effect is found to be present even for a CoO layer as thin as 5 Å.[7] More recent research, both experimental[8,9] and theoretical,[10–12] has focused on the spin structure across the Fe_3O_4-CoO interface. However, little is known about the intrinsic electronic properties of the interface.

In this work, we use epitaxially grown thick Fe_3O_4 (100) films as substrates and then deposit ultrathin CoO (100) films from 1 to 20 ML (monolayer). In this way, we are able to track the evolution of both the structural and electronic properties at the Fe_3O_4-CoO interface as a function of film thickness and examine how the structural and electronic structure at the interface differs from those of bulk Fe_3O_4 and CoO.

II. EXPERIMENTAL DETAILS

The growth and characterization experiments were performed in an interconnected multiple-chamber ultrahigh vacuum (UHV) system consisting of an oxide molecular beam epitaxy (MBE) growth chamber, a sample preparation and analysis chamber, and a chamber equipped with a scanning tunneling microscope. For these experiments, the oxide MBE growth chamber is equipped with reflection-high-energy-electron diffraction (RHEED), one electron beam evaporator (Fe), one high temperature effusion cell (Co), and one standard effusion cell (Mg). A quartz crystal microbalance is used to monitor the evaporation flux from each source. A microwave electron cyclotron resonance (ECR) oxygen plasma source supplies atomic oxygen during growth. The preparation and analysis chamber contains Ar^+-ion bombardment, low-energy-electron diffraction (LEED), He I and He II ultraviolet photoelectron spectroscopy (UPS), Mg $K\alpha$ and Al $K\alpha$ x-ray photoelectron spectroscopy (XPS), and Auger electron spectroscopy (AES), utilizing a cylindrical mirror analyzer. In this work, AES spectra were taken using a primary electron energy of 2 keV, and the peaks were detected by differentiating the energy distribution function [e.g., $dN(E)/dE$].

Since the surface of MgO is very sensitive to H_2O,[13] care must be taken during substrate preparation. The single-crystal MgO (100) substrates (from Princeton Applied Research) were annealed in a dry air flow at around 1000 °C for 10 h before transferring into the UHV chamber. To eliminate surface charging of MgO during UPS spectroscopy, an annular ring of Ni or Co was deposited around the outside of the face of the MgO wafer; this ring was then grounded to the sample holder. (The conductivity of the Fe_3O_4 films grown on top of the MgO was sufficient to leak off surface

charge.) The MgO (100) surface was further prepared by sputtering with 0.5 keV Ar^+ ions for 30 min, annealing in an oxygen plasma at 250 °C for another 30 min, followed by MBE growth of a buffer layer (~180 Å) of MgO.

Fe_3O_4 films were then grown heteroepitaxially on MgO (100), using the procedure that has been perfected by Kim *et al.*,[14] i.e., Fe deposition in oxygen excited by an ECR plasma source, using an O_2 partial pressure of 2×10^{-6} torr, an Fe deposition rate of ~0.6 Å/s, and a substrate temperature of 525 K. The growth conditions for Fe_3O_4 are critical since the film could be either FeO_x if there is insufficient oxygen or Fe_2O_3 if too high an oxygen pressure is used. For the growth of CoO on Fe_3O_4, the control of oxidization is even more critical since not only exposure of the substrate of Fe_3O_4 to O_2 can oxidize it to Fe_2O_3 but also the CoO film could be oxidized to Co_3O_4. The growth rate was maintained at 1 Å/min. Similar to our previous growth of NiO,[3] when growing ultrathin (1–5 ML) CoO films, we first deposit just enough of Co to be oxidized into a monolayer of CoO, and then expose the Co film to 10 L (1 L=10^{-6} torr s) of molecular oxygen; for films beyond 5 ML, Co was deposited in an oxygen ambient of 10 L. The growth was conducted at room temperature. As a standard for comparison to our CoO films, Co_3O_4 was also grown directly on an MgO (100) substrate; in this case, Co was deposited at the same growth rate of 1 Å/min at a growth temperature of 523 K but oxidized with atomic instead of molecular oxygen. An oxygen partial pressure of 1.0×10^{-5} torr was used for the oxygen plasma.

III. RESULTS AND DISCUSSIONS

A. Stoichiometry of Fe_3O_4 and CoO films

The RHEED patterns for the three iron oxides (FeO, Fe_3O_4, and Fe_2O_3) are very different from each other and thus provide a sensitive way to determine the film structure. Figure 1 compares the RHEED patterns of the MgO substrate [(a) and (a′)] and of a 400 Å thick epitaxial Fe_3O_4 film [(b) and (b′)]. The halving of the diffraction line spacing along [110], corresponding to the doubling of the lattice periodicity as Fe_3O_4 grows, is clearly visible. The quarter-order streaks in the zeroth-order zone of the RHEED pattern along [100] correspond to the $(\sqrt{2}x\sqrt{2})$ $R45°$ reconstruction of Fe_3O_4, as verified in the LEED patterns [Figs. 2(a) and 2 (a′)]. These patterns, as well as the XPS spectrum [Fig. 3(a)] of Fe_3O_4 films, are similar to those that we obtained from contamination-free natural single crystals of Fe_3O_4,[3] ruling out the possibility of FeO_x or Fe_2O_3 formation. AES shows that there is no diffusion of Mg into the Fe_3O_4 film. The quality of the Fe_3O_4 films is further verified by transport measurements, which show that the films exhibit the characteristic "Verwey transition" of Fe_3O_4, i.e., the resistance increases abruptly when cooled down to around 122 K.[15] The films also exhibit a giant planar Hall effect, which demonstrates the potential use of magnetite films for nonvolatile magnetic memory applications.[16]

The stoichiometry of the CoO films was also verified by LEED/RHEED patterns and XPS spectra. CoO has the rocksalt structure with a lattice constant of 4.26 Å, whereas

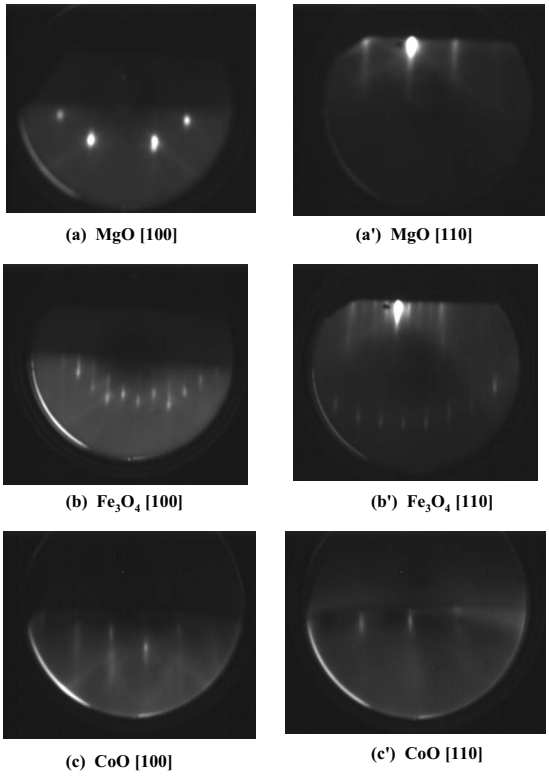

FIG. 1. Typical RHEED patterns [(a) and (a′)] of the MgO (100) substrate, [(b) and (b′)] of Fe_3O_4 (100) films, and [(c) and (c′)] of CoO (100) films, taken along [100] and [110] directions.

Co_3O_4 has a spinel crystal structure (all the Co^{3+} ions are located in the octahedral sites and all the Co^{2+} ions are in the tetrahedral sites),[17] with a lattice constant of 8.09 Å. Figure 2 (h′) shows a LEED pattern of a Co_3O_4 film, which exhibits a (2×2) structure with respect to the surface structure of the single-crystal MgO substrate. Our LEED patterns for the 20 ML CoO film, however, show the 1×1 surface structure [Figs. 2(g) and 2(g′)] of single-crystal CoO.[18] The two-dimensional square phase is further confirmed by the RHEED patterns, where the streak interval increases by a factor of $\sqrt{2}$ when the sample is rotated 45° [Figs. 1(c) and 1 (c′)]. These patterns are similar to those of MgO [Figs. 1(a) and 1(a′)] since CoO and MgO have the same rocksalt structure. As can be seen in Fig. 2, from 2 ML, the LEED pattern has begun to show the features of a thick CoO film. For film thicknesses of 3 ML and greater, the surface symmetry is unchanged, with only an increase in spot intensity.

Figure 3(a) shows the evolution of the Mg $K\alpha$ XPS spectra of the Fe $2p$ and Co $2p$ core levels and the O_{KVV} Auger transitions of the Fe_3O_4 substrate and the CoO films. As the film thickness increases from 1 to 100 ML, the O_{KVV} signals remain constant, but the CoO overlayer attenuates the substrate Fe $2p$ core-level signals; the substrate signal is barely visible beneath 10 ML of CoO. XPS spectra also confirmed the correct stoichiometry of the CoO film. In the Co $2p$ spectra of all the CoO films [Fig. 3(a)], two satellites were observed in addition to the two main peaks from the spin-orbit-split components $2p_{1/2}$ and $2p_{3/2}$. The distance between the main $2p_{1/2}$ peak and its satellite is about 6.3 eV, whereas the

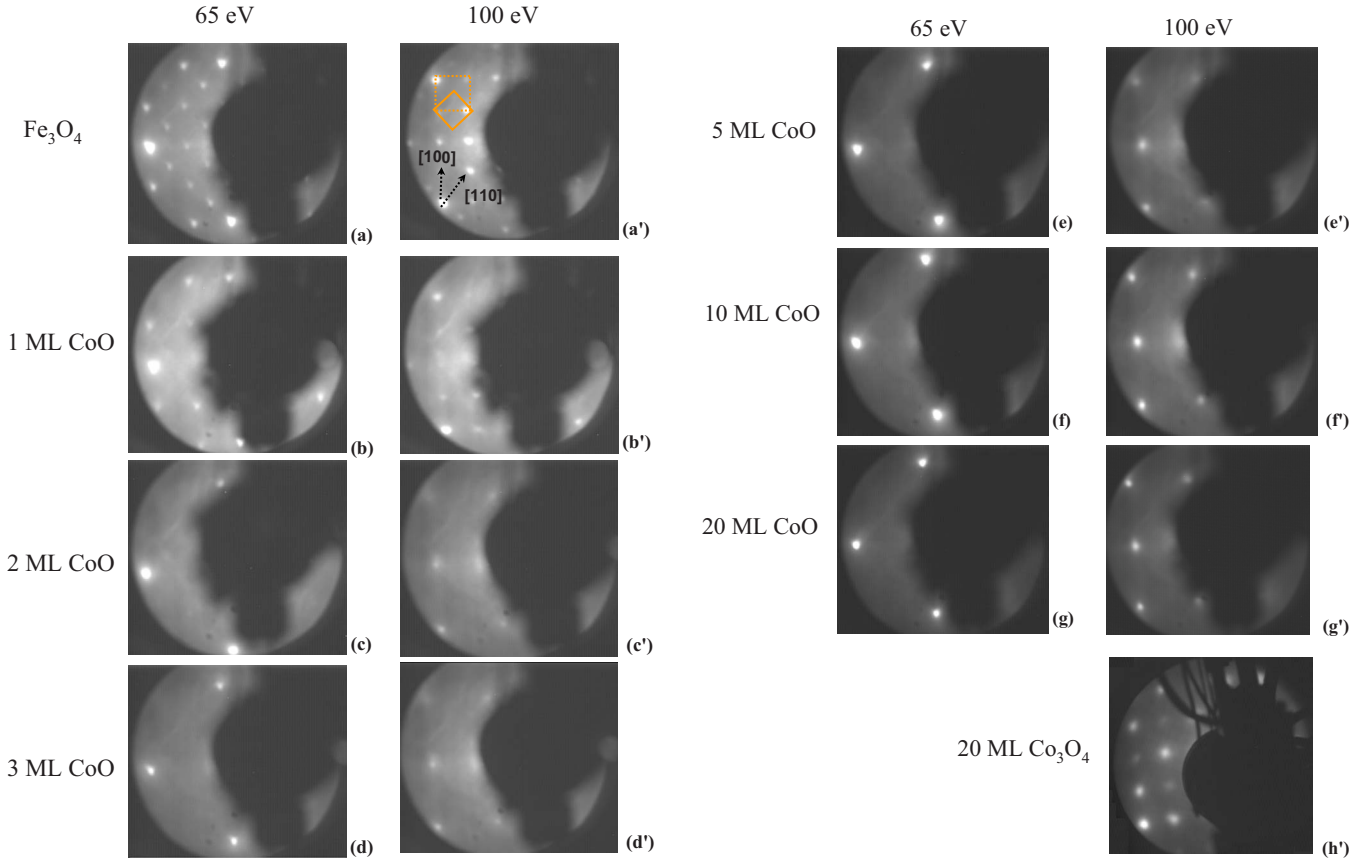

FIG. 2. (Color online) (Left) LEED patterns of Fe_3O_4 (100) and 1–3 ML CoO (100) films, taken with primary energies of [(a)–(d)] 65 eV and [(a′)–(d′)] 100 eV. The p (1×1) unit cell and the $(\sqrt{2}\times\sqrt{2})$ $R45°$ superlattice on the Fe_3O_4 (100) surface are indicated by the dashed square and solid square, respectively. The crystallographic axes are also indicated. (Right) LEED patterns of 5, 10, and 20 ML CoO (100) films, taken with primary energies of [(e)–(g)] 65 eV and [(e′)–(g′)] 100 eV. Also shown is the LEED pattern for a 20 ML Co_3O_4 film taken at (h′) 100 eV.

distance between the main $2p_{3/2}$ peak and its satellite is about 5.9 eV. These values are in agreement with those obtained from CoO powder[19] and cleaved single-crystal CoO (100).[20] If Co_3O_4 were present, we would expect a 10 eV separation of the satellite structures with respect to their main lines.[19,21] No obvious satellites were present in the O 1s core-level spectra [Fig. 3(b)]; the large broad peak located at higher binding energy than the O 1s core level is due to a Co Auger transition.

B. Growth mode of CoO films on Fe_3O_4

The streaky RHEED patterns of CoO films [Figs. 1(c) and 1(c′)] indicate the smoothness of the films. The evolution of the LEED patterns, as well as the XPS core-level spectra, rule out the possibility of a three-dimensional growth mode. The growth mode can be further confirmed from Auger spectra. Figure 4(a) shows an Auger spectrum of the Fe_3O_4 substrate and that of a 20 ML CoO film. The peak energies of 596, 649, and 704 eV correspond to Fe_{LMM}, Fe_{LMV}, and Fe_{LVV} Auger transitions, respectively, whereas Co_{LMM} Auger transitions generate the three peaks at 654, 715, and 775 eV, as well as the two peaks (noted by "☆") near the Fe_{LMM} Auger peak at 596 eV.[22] No Fe_3O_4 Auger peaks are present for a 20 ML CoO film. A quantitative analysis of the attenuation of the substrate Auger signal and the increase of the overlayer Auger signal is presented in Fig. 4(b). The experimental peak-to-peak amplitudes of the Fe 596 eV and Co 775 eV Auger peaks are represented by triangles and squares, respectively. Those two peaks were chosen because they are well separated from other spectral features and are of reasonable intensity. The data points are then fitted using the following formula:[23]

$$I^{\mathrm{Fe}}(m) = I_{\mathrm{O}}^{\mathrm{Fe}} \exp(-md/\lambda_{\mathrm{Fe}}), \tag{1}$$

$$I^{\mathrm{Co}}(m) = I_{\mathrm{O}}^{\mathrm{Co}}[1 - \exp(-md/\lambda_{\mathrm{Co}})], \tag{2}$$

where m is the number of CoO monolayers, with a thickness of d for each monolayer (here, a value of 2.13 Å is used). I_0^{Fe} and I_0^{Co} are the intensities of the clean Fe_3O_4 substrate Auger peak and the 20 ML CoO Auger peak, respectively [Fig. 4(a)]. λ is the inelastic electron mean free path and is the only adjustable parameter; it is chosen to best fit the experimental data, as shown in Fig. 4(b). The fitted curves for Fe (dotted line) and Co (solid line) yield the values of λ_{Fe} =11.1 Å and λ_{Co}=9.4 Å. There values are close to what would be expected from the "universal curve" of electron

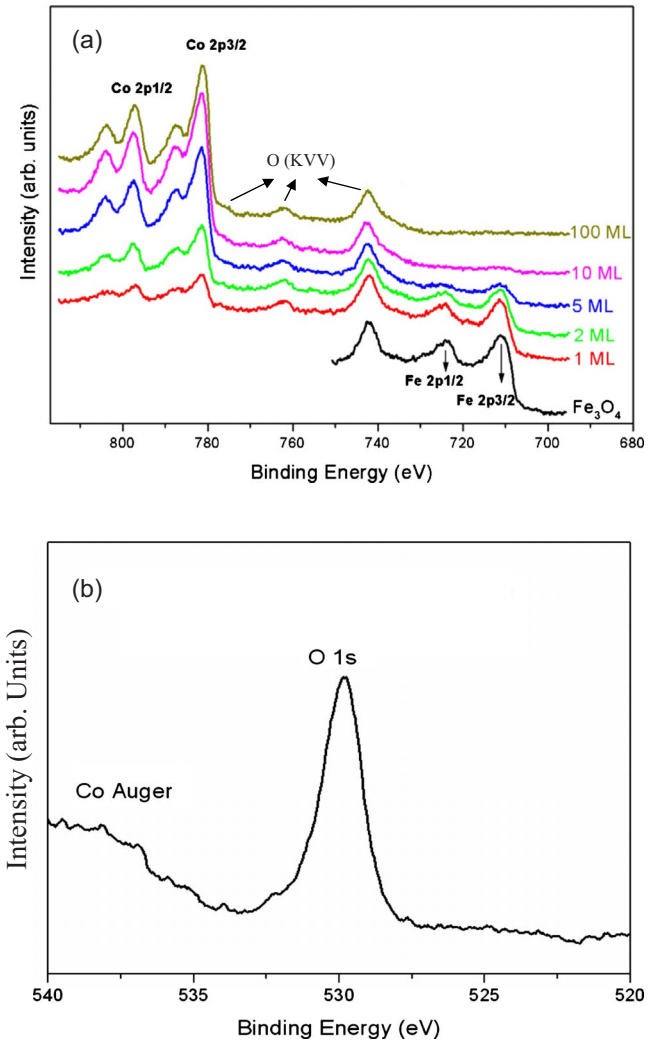

FIG. 3. (Color online) (a) Mg $K\alpha$ XPS spectra of Co $2p$ and Fe $2p$ and Auger spectra of O as 1–100 ML of CoO (100) is grown on Fe_3O_4 (100). (b) Mg $K\alpha$ XPS spectrum of O $1s$ and Auger spectrum of Co from a 20 ML CoO film.

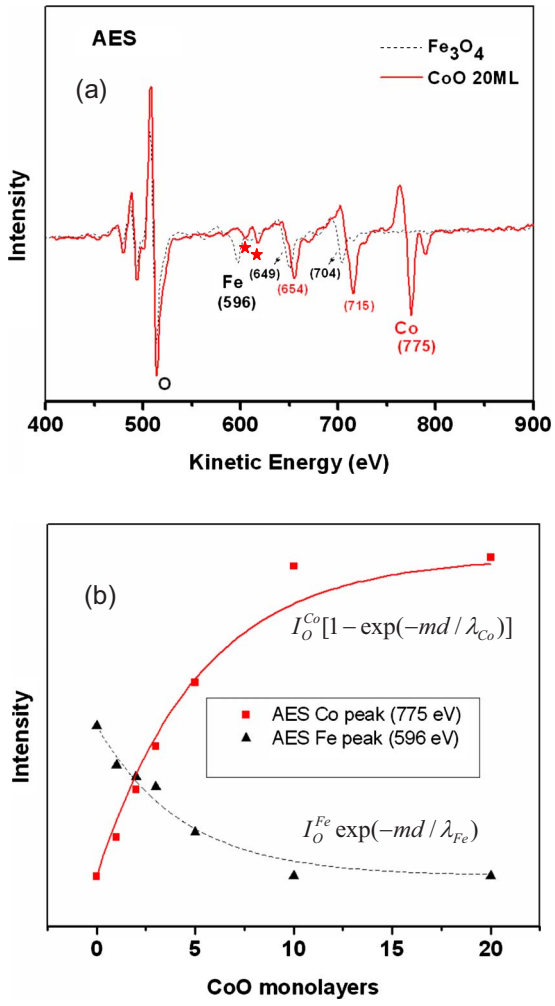

FIG. 4. (Color online) (a) Auger spectra of the Fe_3O_4 substrate and a 20 ML CoO film. The substrate features cannot be seen in the 20 ML CoO spectrum. (b) The AES intensity for Co and Fe peaks as a function of film thickness. The simulation curves (solid for Co and dashed for Fe) agree with the experimental data points (squares for Co and triangles for Fe) (see text for details).

mean free paths in solids.[24] This also indicates a nearly layer-by-layer growth mode.

C. Geometry of the Fe_3O_4-CoO interface

As shown in Fig. 2, the CoO films begin to show bulklike LEED patterns when as thin as 2 ML. For 1 ML, the surface exhibits a (1×1) structure of the Fe_3O_4 substrate, corresponding to a (2×2) superlattice with respect to bulk CoO. Since Co_3O_4 has the same structure as Fe_3O_4, and the LEED pattern of 1 ML CoO [Fig. 2(b′)] is similar to that of Co_3O_4, one might suspect that the 1 ML CoO thin film could have been oxidized to Co_3O_4. This possibility can be ruled out by the XPS spectra. As shown in Fig. 3(a), the core-level Co $2p$ spectrum for the 1 ML film is similar to that of 100 ML CoO but very different from the features for Co_3O_4, as discussed in Sec. III A. The observed LEED pattern for the 1 ML film could originate from the interplay between the overlayer and the substrate.

Because of the extremely close lattice match, CoO (100) grows heteroepitaxially on Fe_3O_4 (100). We can thus speculate about the manner in which the interface might form (see Ref. 3 for a more detailed discussion of this for the similar Fe_3O_4-NiO system). Fe_3O_4 has the complex inverse spinel structure based on a fcc oxygen sublattice. Two-thirds of the Fe cations are Fe^{3+}, with one-half in tetrahedral lattice sites and the other half in octahedral sites; the remaining one-third of the Fe cations are Fe^{2+} occupying octahedral sites. The (100) surface of Fe_3O_4 could be either an A termination containing only half a layer of the tetrahedrally coordinated Fe cations, i.e., the charge neutral "1/2 Fe_{tet}" model,[25] or a B termination composed of oxygen anions and octahedrally coordinated Fe cations with the wavelike pattern that has been calculated to be energetically stable.[26] We therefore discuss the possible interface formation based on those two substrate surfaces and compare them with the LEED observations.

Assuming that the surface is terminated by the 1/2 Fe_{tet} model, there are three types of surface O sites on Fe_3O_4

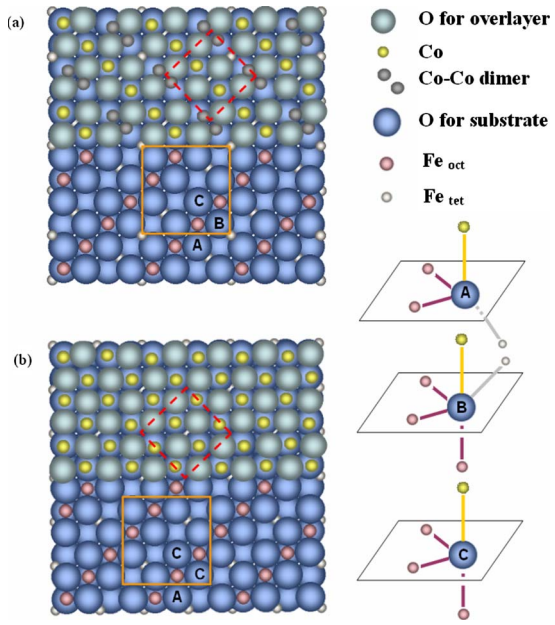

FIG. 5. (Color online) Models for 1 ML CoO on Fe_3O_4 (100) whose surface is (a) terminated by half of the tetrahedral Fe ions or (b) terminated by the distorted oxide layer. For comparison between the substrate and the overlayer, only part of the substrate is covered by CoO in the figures. The solid lines represent the unit cell of a $(\sqrt{2}\times\sqrt{2})$ $R45°$ reconstruction on the Fe_3O_4; the dashed lines indicate the (1×1) unit cell for bulk Fe_3O_4 (a) when Co-Co dimers are formed for the first ML of CoO or (b) when the distortion of the octahedral Fe ions relaxed back to their original position. Both models agree with observed LEED patterns.

(100) [see Fig. 5(a)]; Co ions would sit atop all three O-ion sites, as in the case for Ni ions when NiO is deposited on Fe_3O_4 (100).[3] The "*A*-type" O ion is bound to two octahedral Fe ions within the oxygen plane and one tetrahedral Fe ion in the plane below, as shown in Fig. 5; in this site, the Co is in the same position as an octahedral Fe ion would have been in the bulk magnetite structure. The "*C*-type" O ion is bound to three octahedral Fe ions, two within the oxygen plane and another directly below in the next oxygen plane; in this site, placing a Co atop would complete the four O-cation bonds that are present on every bulk O ion in Fe_3O_4, with possibly different bond angles. The "*B*-type" ion is bound to the same three octahedral Fe ions as the *C*-type ion, but it has an additional bond with a tetrahedral Fe ion on the top plane; placing a Co atop would constitute a fifth O-cation bond to that O ion, as well as creating an extremely short Fe-Co distance of 1.85 Å at the interface. The above model suggests that the interface would reconstruct in some way so as to eliminate the short Fe-Co bond length; one possibility is that the Co on the *B* site would be repelled from the tetrahedral Fe ion and then form a dimer with the Co on the *C* site [Fig. 5(a)]. Such a reconstruction would result in a (1×1) structure of bulk Fe_3O_4, in agreement with the LEED patterns for 1 ML CoO [Figs. 2(b) and 2(b′)]. If the surface were a distorted *B* termination [Fig. 5(b)],[26] then as soon as the first monolayer of CoO was deposited, it should remove the distortion; this could also cause the LEED pattern to go from $(\sqrt{2}x\sqrt{2})$ $R45°$ to (1×1) of bulk Fe_3O_4 for 1 ML CoO [Fig. 5(b)]. In this model, the three types of surface O sites on Fe_3O_4 (100) mentioned above reduce to two, types *A* and *C*; types *B* and *C* become the same. When Co is placed atop an O anion, each O site would form four O-cation bonds as in bulk Fe_3O_4; however, the bond angles for the two *C* sites could still be different since Co is not in the same position as an octahedral Fe ion would have been in the bulk magnetite structure. Therefore, we cannot distinguish the two possibilities from the observed LEED patterns.

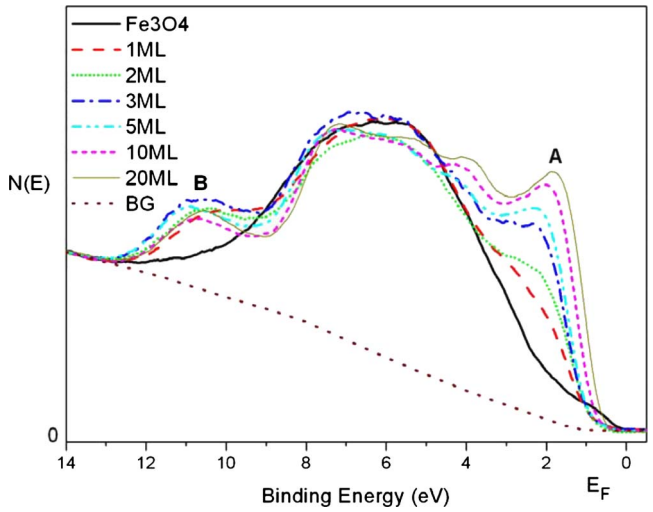

FIG. 6. (Color online) He II UPS spectra for CoO films grown on Fe_3O_4. Peaks *A* and *B* are associated with the Co 3*d* [specifically $3d^7$ (L)] emission and its satellite; the peaks in between are primarily O 2*p*-derived states (Ref. 29). The dotted curve underneath the spectra indicates an integral inelastic Li background function (Ref. 30).

D. Electronic properties of the Fe_3O_4-CoO interface

1. Band shift

Figure 6 shows the evolution of He II UPS spectra as a function of CoO layer thickness; each spectrum has been corrected for additional lines in the He discharge lamp.[27] In the Fe_3O_4 spectra, the broad feature between 3 and 12 eV binding energy consists of hybridized O 2*p*–Fe 3*d* orbitals; the shoulder of emission between 3 eV and E_F is due primarily to the $3d^6$ electronic configuration of the Fe^{2+} ions. The finite emission very close to E_F shows the weakly metallic nature of Fe_3O_4. The features in the spectrum of the 20 ML film that are most distinguishable from those of the substrate Fe_3O_4 are the five peaks located between 2 and 11 eV below E_F; these are hybridized O 2*p*–Co 3*d* orbitals, in agreement with the data from cleaved single-crystal CoO (100) surfaces.[28,29] Peaks *A* and *B* are associated with the Co 3*d* [specifically $3d^7$ (L)] emission and its satellite; the peaks in between are primarily O 2*p*-derived states.[29] For thinner CoO films, the valence band maxima in the UPS spectra were found to shift by up to 0.42 eV toward higher binding energy, similar to what we observed for the growth of NiO films on the same substrate.[3] The shift is more obvious when

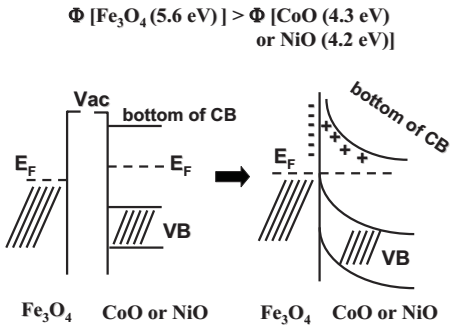

FIG. 7. Band bending at the interfaces of Fe_3O_4-CoO and Fe_3O_4-NiO, based on the Schottky barrier model (Ref. 33).

an inelastic Li background[30] (as in Fig. 6) has been subtracted from each spectrum (not shown). [The background function used is a Li background, which is described in Ref. 30. Unlike the integral (or Shirley) background appropriate for higher photon energy XPS, the Li background explicitly includes the secondary-electron cascade process and gives a much better fit to the background for UPS photon energies. Reference 30 gives examples for several metal oxides.]

When greater-than-band-gap light incident on a sample is too intense for the photoinduced charges on the surface to leak off completely, it will result in the so-called "surface photovoltage," which has been found to cause band shifts.[31] To examine whether the origin of this band shift is related to the intensity of the UV light, we took UPS spectra for different helium pressures. The helium discharge lamp emits most of its UV radiation at 21.2 eV (He I) and only a small amount of radiation at 40.8 eV (He II), the photon energy that we normally use to take UPS spectra. The total intensity of the UV radiation from the lamp increases proportional to helium pressure in the lamp. We took He II spectra at helium pressures of 1.2 and 1.8 torr, as well as He I spectra at 3.0 torr. (At a lamp pressure of 3 torr, the He II intensity, which decreases rapidly with increasing He pressure, is too small to be useful.) We found that all the data exhibit about the same band shift, regardless of the UV light intensity. Thus, surface photovoltage is not the cause of the band shift.

This band shift, which occurs for both CoO films in this work and NiO films in our previous report,[3] is not due to surface charging either since it would only occur for thicker films (for ultrathin films, electrons can tunnel from the metallic substrate to neutralize excess surface charge) and it would have shifted spectra to higher apparent binding energy for thicker films, opposite to our observations. The shift is probably not caused by band bending at the metal-insulator interface either since the work function of Fe_3O_4 (100) (5.3 eV) (Ref. 26) is larger than that of CoO (100) (4.3 eV) (Ref. 32) and NiO (100) (4.2 eV),[32] and a simple Schottky barrier model (Fig. 7) (Ref. 33) would then predict a band shift opposite to that observed.

The origin of the band shift might relate to the strong electron correlation present in CoO and NiO films. In strongly correlated oxides, the electronic structure is determined by several important quantities, e.g., on-site Coulomb interactions U, charge transfer energy Δ, and electron bandwidth W.[34] The values U and Δ are found to be modified when oxides are scaled down to thin films grown on conductors; this could potentially change the band gap of the films. For example, Altieri *et al.*[35] performed XPS experiments on MgO films grown on the Ag (100) surface and found that their U and Δ values were changed from the bulk values for very thin films. These modifications were attributed to a combination of the image potential of the ionic charges in the film generated in the metallic substrate and an effect of opposite sign associated with the polarization energy loss due to the reduced ligand coordination near the interface. In our case, both CoO and NiO films[3] are deposited on a conducting Fe_3O_4 substrate. Although Fe_3O_4 (100) cannot be treated as a simple jellium metal surface as was Ag, values of the U and Δ for CoO and NiO could also change, due to the image potential and the polarization energy, and thus cause the band shift that we have observed. However, if that were the case, we would expect a larger band shift for thinner films and smaller shift for the bulklike 10 or 20 ML films. This is not what we observed for either CoO or NiO films.

The band shift could be due to the difference of electronic structure between the thin CoO or NiO film and bulk CoO or NiO. For these insulating materials, the Fermi level of the sample lies somewhere in the band gap and is not pinned at a specific energy as it is in metals. Thus, small differences in the properties of the sample or its surface, as can occur during the growth of ultrathin films, can change the position of E_F by a significant amount. (This issue is addressed in depth in Ref. 36, where examples are given for metal oxides.) Since UPS spectra are referenced to a common Fermi energy, this effect appears as a relative energy shift between different spectra. When UPS spectra are subtracted from one another, as is done in the analysis below, such a shift results in spurious features in the difference spectra that are not related to any other properties of the spectra. [Such features can be very large in spectral regions such as band edges where the slope of the spectra are large; an example of such residual artifacts that could not be completely removed can be seen as the small, narrow feature at about 1 eV binding energy in the difference spectra of Fig. 8(c) below.] Even when such band shifts are present, however, useful information can be obtained from difference spectra if the UPS spectra are aligned in energy before subtraction.[36] In the analysis below, the UPS spectra were aligned at the upper edge of the valence band for the thickest films before taking differences.

2. Interface states

a. Ultraviolet photoelectron spectroscopy modeling without interface states. Since UPS spectra sample several monolayers below the surface of a sample, spectra measured for ultrathin films deposited onto a substrate will consist of a superposition of emission from the substrate, any interfacial states that may be present, and the overlayer film, with each weighted by electron escape depths. Assuming layer-by-layer growth, the spectral intensity I as a function of thin film thickness d, if no interface electronic states were present, is given by

$$I(d) = I_0^{Fe_3O_4} \exp(-d/\lambda) + I_0^{CoO}[1 - \exp(-d/\lambda)], \qquad (3)$$

where $I_0^{Fe_3O_4}$ and I_0^{CoO} are the UPS spectra for semi-infinite samples of each material. Differences between measured

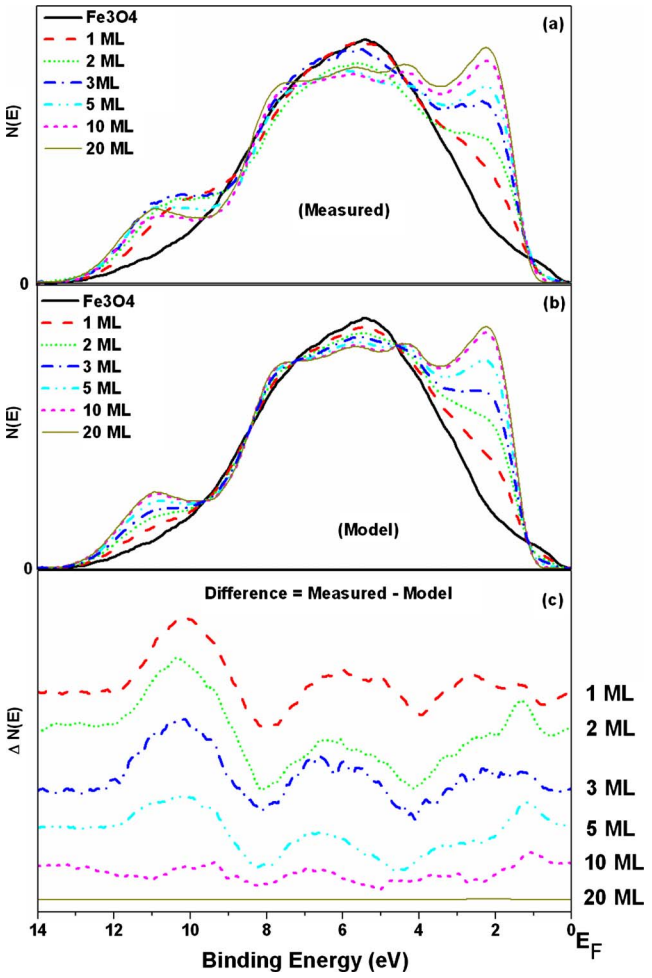

FIG. 8. (Color online) (a) UPS spectra of Fig. 6 after the alignment of the Co 3*d* peak near the Fermi level and the subtraction of an inelastic background. (b) Model spectra for (a), assuming no interface states. (c) Difference spectra between (a) experimental and (b) model spectra, separated for clarity.

UPS spectra and the above model may then result from the interfacial electronic structure.

Figure 8(a) shows the UPS spectra of Fig. 6 after the subtraction of the inelastic background. We simulated the experimental data with the simple additive model given by Eq. (3); the results are shown in Fig. 8(b). The experimental clean Fe_3O_4 substrate spectrum and the 20 ML CoO spectrum were taken as the respective bulk spectra, $I_0^{Fe_3O_4}$ and I_0^{CoO}. In order to accurately determine the changes in the UPS spectra for CoO films of different thicknesses, the experimental UPS spectra for the clean Fe_3O_4 substrate and the thickest CoO film from each experimental run were used for $I_0^{Fe_3O_4}$ and I_0^{CoO} in the analysis of that run. In addition, since slight differences in the position of the sample in front of the spectrometer can give slightly different UPS spectra (due to photoelectron diffraction effects, etc.), the substrate was positioned in front of the electron spectrometer and not moved during CoO growth. A value of 6.4 Å for λ was determined from the best fit of the attenuation of the Co 3*d* peak at 2 eV to $[1-\exp(-d/\lambda)]$ Figure 8(c) presents difference spectra in which the model spectra [Fig. 8(b)] have been subtracted from the experimental ones [Fig. 8(a)]. It can be seen that there are three main peaks in the difference spectra. These three features show up even when the inelastic background is included in Figs. 8(a) and 8(b). These features could originate from interface states.

b. Sequential differences from ultraviolet photoelectron spectroscopy spectra. Two approaches have been used to confirm that interface states are present and to determine their UPS spectra. The first is simply to take sequential differences between the experimental UPS spectra as CoO layers are deposited onto the Fe_3O_4. The purpose is to separate out the electronic structure of each CoO layer by subtracting from it the intensity due to the background, the substrate Fe_3O_4, and the CoO layers underneath. Assuming that the *j*th NiO layer is grown on top of the *i*th layer, the equation,

$$I_{j\text{th}} = I_j - I_i \exp(-d_j/\lambda), \tag{4}$$

yields the intensity from only the *j*th layer, which has thickness d_j. I_j and I_i represent the total intensities from the sample after the *j*th and the *i*th films are grown, respectively. Thus, for the data in Fig. 9(a), the "fourth+fifth" layer difference spectrum is obtained by subtracting the 3 ML spectrum from the 5 ML one in Fig. 8(a), with $d_j=2$ ML; the third layer spectrum is obtained by subtracting the 2 ML spectrum from the 3 ML one, with $d_j=1$ ML, etc. The first layer spectrum is obtained by subtracting the substrate spectrum, with $d_j=1$ ML. The intensity of each resultant spectrum is then normalized to the bulklike 20 ML film, as shown in Fig. 9(b). Figure 9(c) shows the difference between each spectrum in Fig. 9(a) and the bulklike spectrum in Fig. 9(b). It can be seen that, from the second monolayer of CoO, the spectra are nearly identical to bulklike CoO. However, the features in the first monolayer of the film are very different, especially around a binding energy of 10 eV. (An implicit assumption in this procedure is that each additional CoO layer does not perturb the electronic structure of the layers beneath it; this assumption will be relaxed in the analysis procedures described below.)

c. Ultraviolet photoelectron spectroscopy modeling with interface states. Our second approach is to use a specific model for the extent of the interfacial region and to model the resulting UPS spectra, including interface states. Fe_3O_4 is weakly metallic, while CoO is an insulator with a band gap of about 6 eV.[37] In general, the electronic states at a metal-insulator interface are more likely to extend farther into the metal than into the insulator.[38] Because of the large band gap of CoO, the interface states here most likely involve primarily the first ML of CoO, although they could extend a bit farther into the Fe_3O_4. (The sequential difference spectra described in Sec. III D 2 b are consistent with that assumption.) We thus construct a model assuming that the interface states involve only the first monolayer of CoO plus the top monolayer of the Fe_3O_4 substrate, making the total interface layer 2 ML thick [Fig. 10(a)]. (While it is possible that the interface states extend deeper than 1 ML into the Fe_3O_4 substrate,

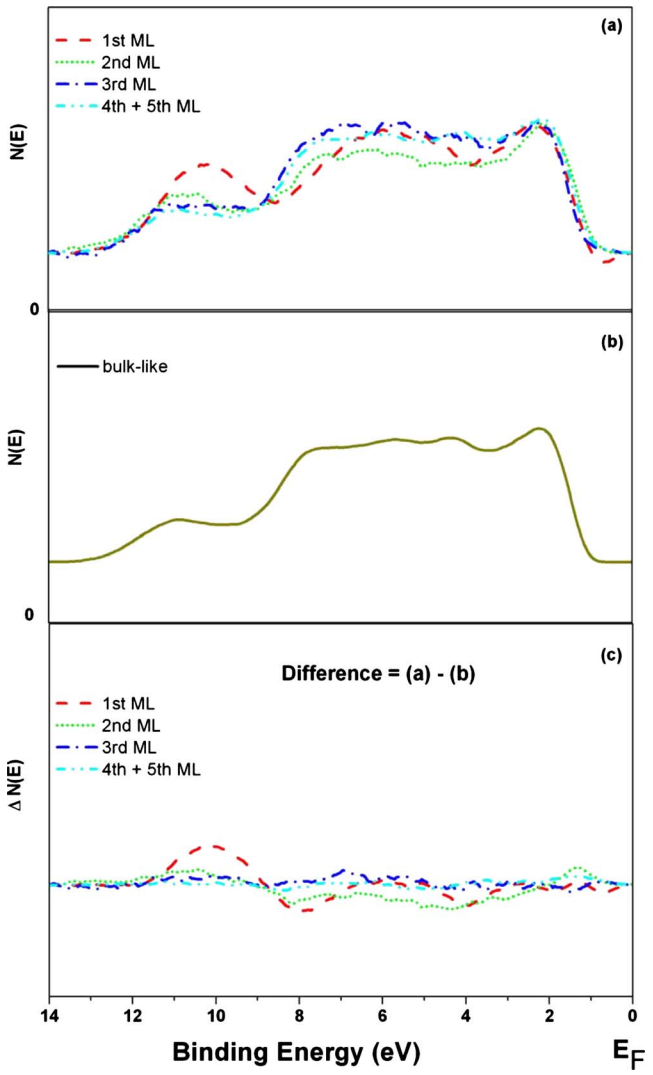

FIG. 9. (Color online) (a) Sequential differences taken from the data in Fig. 8(a). The intensities have been normalized to the bulklike 20 ML CoO spectrum in (b). (c) shows the difference between each spectrum in (a) and the bulklike spectrum in (b).

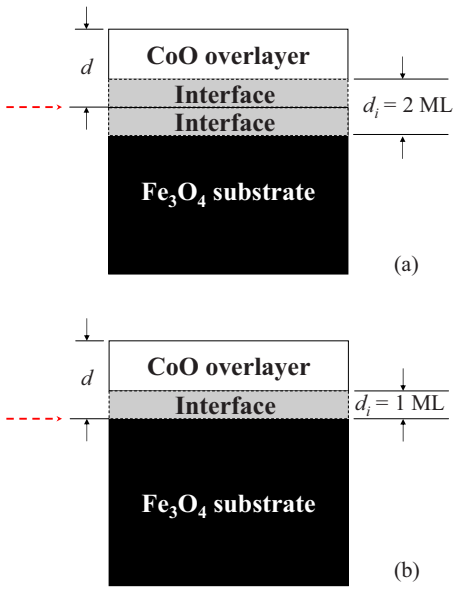

FIG. 10. (Color online) Two models of interfacial electronic states. The interface states in (a) involve 1 ML of CoO and the first ML of the Fe_3O_4 substrate, while those in (b) involve only 1 ML of CoO. d is the total thickness of CoO deposited and d_i is the interface layer thickness. The dashed arrows indicate the stoichiometric Fe_3O_4/CoO interface.

that would make only minor differences in the results obtained below from this model.) When interface states are included, the modeling of the spectral intensity I' as a function of thin film thickness d is given by

$$I'(d) = I_0^{Fe_3O_4}\exp[-(d+d_{is})/\lambda] + I_0^{CoO}\{1-\exp[-(d-d_{i0})/\lambda]\} + I_0^{interface}[1-\exp(-d_i/\lambda)]\exp[-(d-d_{i0})/\lambda]. \quad (5)$$

The model difference spectra $\Delta I(d)$ can be obtained by subtracting $I(d)$ in Eq. (3) from $I'(d)$ in Eq. (5),

$$\Delta I(d) = I_0^{Fe_3O_4}\exp(-d/\lambda)[\exp(-d_{is}/\lambda)-1] + I_0^{CoO}\exp(-d/\lambda)\ [1-\exp(d_{i0}/\lambda)]\} + I_0^{interface}[1-\exp(-d_i/\lambda)]\exp[-(d-d_{i0})/\lambda]. \quad (6)$$

$\Delta I(d)$ is now the difference between the model spectra with interface states and the model spectra without interface states. Since the spectra in Fig. 8(c) represent the difference between the experimental spectra and the model spectra without interface states, with the assumption that the experimental spectra contain interface states, we can use the difference spectra in Fig. 8(c) as $\Delta I(d)$. Then, the interface state spectra $I_0^{interface}$ can be determined from

$$I_0^{interface} = \frac{\Delta I(d) - I_0^{Fe_3O_4}\exp(-d/\lambda)[\exp(-d_{is}/\lambda)-1] - I_0^{CoO}\exp(-d/\lambda)\ [1-\exp(d_{i0}/\lambda)]\}}{[1-\exp(-d_i/\lambda)]\exp[-(d-d_{i0})/\lambda]}. \quad (7)$$

For the model proposed in Fig. 10(a), $d_{is}=d_{i0}=1$ ML and $d_i=2$ ML, Eq. (7) becomes

$$I_{01}^{interface} = \frac{\Delta I(d) - I_0^{Fe_3O_4}\exp(-d/\lambda)\{\exp[-(d_i/2)/\lambda]-1\} - I_0^{CoO}\exp(-d/\lambda)\{1-\exp[(d_i/2)/\lambda]\}}{[1-\exp(-d_i/\lambda)]\exp[-(d-d_i/2)/\lambda]}. \quad (8)$$

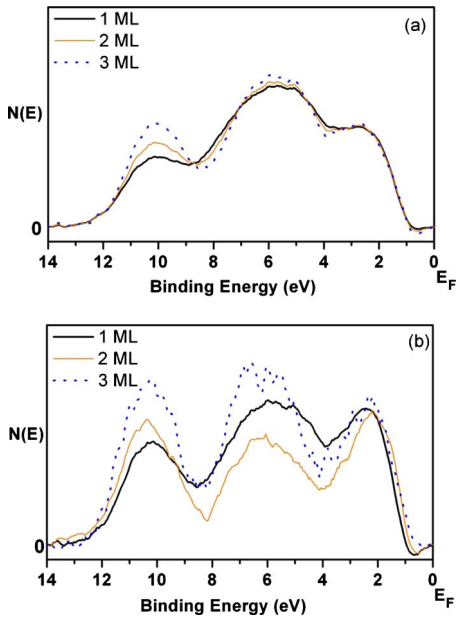

FIG. 11. (Color online) The calculated UPS spectra for interface states $I_0^{\text{interface}}$ for the two interface models in Figs. 10(a) and 10(b), respectively (see text for details).

The calculated $I_{01}^{\text{interface}}$ spectra are shown in Fig. 11(a) using the difference spectra $\Delta I(d)$ in Fig. 8(c) (only the spectra of $d=1$, 2, and 3 ML are used because they have more clearly discernible features). It can be seen that these three $I_{01}^{\text{interface}}$ spectra are very similar to each other. This suggests that the interface model in Fig. 10(a) is very close to the actual case.

As a check on the above model, we calculated a new set of $I_{02}^{\text{interface}}$ spectra using the model shown in Fig. 10(b). In that model, the interface is assumed to involve only the first ML of CoO, without extending into the Fe_3O_4 substrate. Thus, $d_{is}=0$, $d_{i0}=d_i=1$ ML, and Eq. (7) becomes

$$I_{02}^{\text{interface}} = \frac{\Delta I(d) - I_0^{\text{CO}} \exp(-d/\lambda)[1-\exp(d_i/\lambda)]}{[1-\exp(-d_i/\lambda)]\exp[-(d-d_i)/\lambda]}. \quad (9)$$

The calculated $I_{02}^{\text{interface}}$ spectra are plotted in Fig. 11(b). The three interface spectra that result are quite different from each other, unlike the case for the $I_{01}^{\text{interface}}$ spectra in Fig. 11(a). Thus, the first interface model in Fig. 10(a) gives better values for d_{is}, d_{i0}, d_i, and $I_0^{\text{interface}}$ than does the second model.

The average of the calculated UPS $I_{01}^{\text{interface}}$ spectra in Fig. 11(a) is our best estimate of the electronic structure at the Fe_3O_4-CoO interface. Figure 12 compares that interface state spectrum (thick solid curve) to the spectra of the Fe_3O_4 substrate (thin solid curve) and the bulklike CoO film (dashed curve). The interface spectrum is significantly different from those of either the substrate or the overlayer, with three main

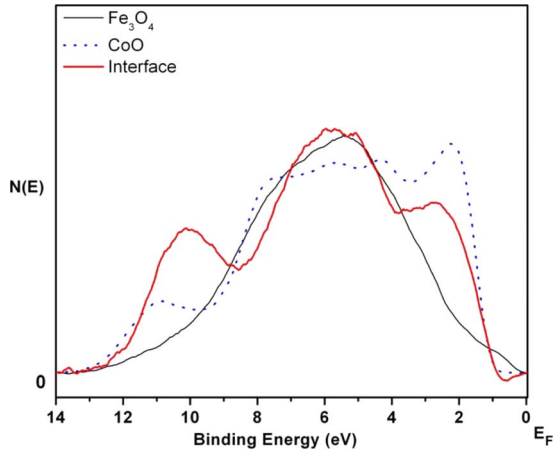

FIG. 12. (Color online) Comparison of the spectra for the Fe_3O_4 substrate, the thickest CoO film [both from Fig. 8(a)], and the interface electron state, averaged from the three spectra in Fig. 11(a).

peaks located at energies of about 10, 5.5, and 2.5 eV. These interface electronic states could originate from a bonding configuration at the interface that is different from those in the substrate and the overlayer, as shown in Fig. 5.

Our results indicate a promising probe to identify embedded interface electronic states using UPS spectra. However, it is important to keep several points in mind when using this method. The application of Eqs.(1)–(9) assumes a layer-by-layer growth mode; if three-dimensional islands are present, the equations are no longer strictly valid. Since any band shift has a profound effect on the differences taken between experimental and model photoemission spectra, the validity of the analysis requires the correct treatment of band shifts. Also, the use of UPS requires that at least the substrate has to be sufficiently electrically conducting that the sample surface will remain at a constant potential. In the case of an insulating substrate, aids such as an electron flood gun would be needed for charge compensation.

IV. SUMMARY

LEED, RHEED, XPS, and AES are applied to investigate the stoichiometry and the growth mode of Fe_3O_4 (100) films deposited onto single-crystal MgO (100), as well as CoO (100) films grown on Fe_3O_4 (100). Two models for the atomic structure of the interface are proposed based on two different models of the substrate surface structure; both models are found to be consistent with the measured LEED patterns. In addition, we have performed UPS experiments on CoO (100) films grown on Fe_3O_4 (100). We observed a shift of the valence band maximum relative to E_F for ultrathin CoO films. When the evolution of the density of states in the O $2p$/Fe $3d$/Co $3d$ band as a function of overlayer thickness observed in UPS is compared to the UPS spectra that are predicted for various models of interface structure, electronic states at the Fe_3O_4-CoO interface can be identified. A structural model of the interface is also proposed.

ACKNOWLEDGMENTS

This research is partially supported by the U.S. Department of Energy Grant No. DE-FG02-00ER45844, NSF Equipment Grant No. DMR-0075824, and NSF Grant No. MRSEC DMR-0520495. The authors also thank J.-B. Yau for performing transport measurements to verify the Verwey transition of the Fe_3O_4 films, and W. Gao, M. Li, J. Wang, and C. A. F. Vaz for the assistance in the laboratory.

[1] P. J. van der Zaag, P. J. H. Bloemen, J. M. Gaines, R. M. Wolf, P. A. A. van der Heijden, R. J. M. van de Veerdonk, and W. J. M. de Jonge, J. Magn. Magn. Mater. **211**, 301 (2000).
[2] T. B. Reed, *Free Energy of Formation of Binary Compounds* (MIT, Cambridge, MA, 1971).
[3] H. Q. Wang, W. Gao, E. I. Altman, and V. E. Henrich, J. Vac. Sci. Technol. A **22**, 1675 (2004).
[4] T. Terashima and Y. Bando, Thin Solid Films **152**, 455 (1987).
[5] R. M. Wolf, A. E. M. De Veirman, P. van der Sluis, P. J. van der Zaag, and J. B. F. aan de Stegge, *Epitaxial Oxide Thin Films and Heterostructures*, MRS Symposia Proceedings No. 341 (Materials Research Society, Pittsburgh, 1994), p. 23.
[6] P. A. A. van der Heijden, C. H. W. Swüste, W. J. M. de Jonge, J. M. Gaines, J. T. W. M. van Eemeren, and K. M. Schep, Phys. Rev. Lett. **82**, 1020 (1999); J. A. Borchers, Y. Ijiri, D. M. Lind, P. G. Ivanov, R. W. Erwin, S. H. Lee, and C. F. Majkrzak, J. Appl. Phys. **85**, 5883 (1999); J. A. Borchers, Y. Ijiri, D. M. Lind, P. G. Ivanov, R. W. Erwin, A. Qasba, S. H. Lee, K. V. O'Donovan, and D. C. Dender, Appl. Phys. Lett. **77**, 4187 (2000).
[7] P. J. van der Zaag, A. R. Ball, L. F. Feiner, R. M. Wolf, and P. A. A. van der Heijden, J. Appl. Phys. **79**, 5103 (1996).
[8] P. J. van der Zaag, Y. Ijiri, J. A. Borchers, L. F. Feiner, R. M. Wolf, J. M. Gaines, R. W. Erwin, and M. A. Verheijen, Phys. Rev. Lett. **84**, 6102 (2000).
[9] Y. Ijiri, T. C. Schulthess, J. A. Borchers, P. J. van der Zaag, and R. W. Erwin, Phys. Rev. Lett. **99**, 147201 (2007).
[10] T. J. Moran, J. Nogues, D. Lederman, and I. K. Schuller, Appl. Phys. Lett. **72**, 617 (1998).
[11] N. C. Koon, Phys. Rev. Lett. **78**, 4865 (1997).
[12] S.-H. Tsai, D. P. Landau, and T. C. Schulthess, J. Appl. Phys. **91**, 6884 (2002).
[13] D. A. Shockey and G. W. Groves, J. Am. Ceram. Soc. **51**, 299 (1968).
[14] Y. J. Kim, Y. Gao, and S. A. Chambers, Surf. Sci. **371**, 358 (1997).
[15] E. J. W. Verwey, Nature (London) **144**, 327 (1931); E. J. W. Verwey and P. W. Haayman, Physica (Utrecht) **8**, 979 (1941); E. J. W. Verwey, P. W. Haayman, and F. C. Romeijan, J. Chem. Phys. **15**, 181 (1947).
[16] Y. Bason, L. Klein, H. Q. Wang, J. Hoffman, X. Hong, V. E. Henrich, and C. H. Ahn, J. Appl. Phys. **101**, 09J507 (2007).
[17] M. A. Langell, M. D. Anderson, G. A. Carson, L. Peng, and S. Smith, Phys. Rev. B **59**, 4791 (1999).
[18] G. A. Carson, M. H. Nassir, and M. A. Langell, J. Vac. Sci. Technol. A **14**, 1637 (1996).
[19] T. J. Chuang, C. R. Brundle, and D. W. Rice, Surf. Sci. **59**, 413 (1976).
[20] Z. X. Shen, J. W. Allen, P. A. P. Lindberg, D. S. Dessau, B. O. Wells, A. Borg, W. Ellis, J. S. Kang, S.-J. Oh, I. Lindau, and W. E. Spicer, Phys. Rev. B **42**, 1817 (1990).
[21] D. C. Frost, C. A. McDowell, and J. S. Woolsey, Mol. Phys. **27**, 1473 (1974).
[22] C. D. Wagner, W. M. Riggs, L. E. Davis, and J. F. Moulder, in *Handbook of X-ray Photoelectron Spectroscopy*, edited by G. E. Muilenberg (Perkin-Elmer, Eden Prairie, 1979).
[23] C. C. Chang, Surf. Sci. **48**, 9 (1975).
[24] M. P. Seah and W. A. Dench, Surf. Interface Anal. **1**, 2 (1979).
[25] H. Q. Wang, E. I. Altman, and V. E. Henrich, Phys. Rev. B **73**, 235418 (2006) and references therein.
[26] R. Pentcheva, F. Wendler, H. L. Meyerheim, W. Moritz, N. Jedrecy, and M. Scheffler, Phys. Rev. Lett. **94**, 126101 (2005).
[27] J. W. Rabalais, *Principles of Ultraviolet Photoelectron Spectroscopy* (Wiley, New York, 1977); J. H. D. Eland, *Photoelectron Spectroscopy*, 2nd. ed (Butterworths, London, 1984).
[28] J. L. Mackay and V. E. Henrich, Phys. Rev. B **39**, 6156 (1989).
[29] Z. X. Shen, J. W. Allen, P. A. P. Lindberg, D. S. Dessau, B. O. Wells, A. Borg, W. Ellis, J. S. Kang, S.-J. Oh, I. Lindau, and W. E. Spicer, Phys. Rev. B **42**, 1817 (1990).
[30] X. Li, Z. Zhang, and V. E. Henrich, J. Electron Spectrosc. Relat. Phenom. **63**, 253 (1993).
[31] D. K. Schroder, Meas. Sci. Technol. **12**, R16 (2001).
[32] V. E. Henrich and P. A. Cox, *The Surface Science of Metal Oxides* (Cambridge University Press, Cambridge, 1994).
[33] Modified from C. Kittle, *Introduction to Solid State Physics*, 7th ed. (Wiley, New York, 1996).
[34] S. Altieri, L. H. Tjeng, and G. A. Sawatzky, Thin Solid Films **400**, 9 (2001).
[35] S. Altieri, L. H. Tjeng, F. C. Voogt, T. Hibma, and G. A. Sawatzky, Phys. Rev. B **59**, R2517 (1999).
[36] V. E. Henrich, Surf. Sci. **284**, 200 (1993).
[37] R. J. Powell and W. E. Spicer, Phys. Rev. B **2**, 2182 (1970).
[38] S. Ismail-Beigi (private communication).